Multiple phase coexistence in finite systems

Ralph E. Kunz* and R. Stephen Berry
Department of Chemistry and the James Franck Institute, The University of Chicago, Chicago, Illinois 60637
(Received 9 August 1993)

Dynamic coexistence of several phaselike forms, a solid, microcrystalline phase, a homogeneously melted phase, and phases exhibiting a solid core and a melted surface, is found in isothermal molecular-dynamics simulations of magic-number rare-gas clusters. We present a theoretical model for the equilibrium and dynamics of phases of small systems that incorporates homogeneous *and* heterogeneous phases and gives necessary conditions for the material parameters if a cluster is to exhibit the observed multiple-phase behavior.

PACS number(s): 64.60.My, 05.70.Fh, 36.40.+d, 64.70.Dv

I. INTRODUCTION

The melting-freezing phase transition of small systems, notably clusters and nanophase materials, has attracted increasing interest both experimentally [1,2] and theoretically [3–6], its main motivation lying in connecting the dynamics of isomerism at the molecular level to the familiar macroscopic phase transition. A theoretical framework was developed [3,4,7–9] and substantiated by simulation models carried out with Lennard-Jones [6,10–15] Morse [16], and alkali-halide (Born-Mayer and shielded Coulomb) potentials [18]. This work indicated that clusters may exhibit sharp but unequal limiting temperatures for freezing and melting. Its most immediate consequence is that clusters showing this behavior have a finite range of temperature and pressure within which solid and liquid clusters of a specific size may coexist. Within this band of temperatures the ratio of solidlike and liquidlike forms changes smoothly. This obviously differs from bulk matter, whose freezing-melting transition occurs sharply at a single temperature for each pressure. The theory of this phenomenon, as presented until now, is restricted to changes between homogeneous phases and does not recognize behavior with heterogeneous phases such as surface-melted [17] or nonwetted structures [18].

Similarly, the concept of surface melting has grown into an area of mounting attention both on the experimental [19] and theoretical [20–27] sides, its origin stemming partly from the quest to explain the nonexistence of superheated solids. Whereas most of the previous work concentrated on bulk systems (or small systems that could be treated as infinite), work on surface phenomena in small systems such as clusters with three to several hundreds of atoms is relatively uncommon. Briant and Burton [28] had proposed the idea of surface melting as early as 1975 and Nauchitel and Pertsin [29] found evidence for it in Monte Carlo simulations of Ar_{55} in 1980. In a study of Ar_N, $N=40-147$, and Cu_{55} clusters Cheng and Berry [17] report surface melting at temperatures below the onset of homogeneous melting on the basis of isoergic molecular-dynamics (MD) simulations and propose a mechanism for the process.

The occurrence of coexistence phenomena [29,30] and surface melting [17] in different accounts of the same argon clusters raises the question of what role surface melting has in phase changes of clusters. In terms of a different emphasis, the occurrence of surface melting calls for a generalization of the theory, henceforth allowing for heterogeneous phases to enter.

Based on these two considerations we have organized our study and this paper. In Sec. II we report the results of isothermal MD simulations of Ar_{55} and Ar_{147} clusters in a temperature range in which surface and homogeneous melting are possible. Building upon the results from these computer experiments we devise a simple melting theory in Sec. III, expanding the validity range of a model by Wales and Berry [4] that describes the coexistence of homogeneous phases, by including heterogeneous phases as well. In Sec. IV we discuss the results and draw the conclusions in Sec. V.

II. NUMERICAL SIMULATIONS

A. Methods

To investigate the phase coexistence behavior of clusters we have chosen to conduct constant-temperature MD simulations of Ar_{55} and Ar_{147} clusters. As is frequently done, their potential energy ϕ was modeled by a pairwise interaction given by the Lennard-Jones potential

$$\phi(\mathbf{r}_1,\ldots,\mathbf{r}_N)=4\varepsilon\sum_{i<j}\left[\left[\frac{\sigma}{\mathbf{r}_i-\mathbf{r}_j}\right]^{12}-\left[\frac{\sigma}{\mathbf{r}_i-\mathbf{r}_j}\right]^{6}\right], \quad (1)$$

where $\varepsilon=1.67\times10^{-7}$ J and $\sigma=3.4$ Å are widely used parameters for argon.

The equations of motion we used for the constant-temperature MD runs are those given by Nosé [31,32]. By adding a suitable pair of canonical variables to the classical Hamiltonian equations governing the motion of the atoms, we describe the dynamics of the N-particle system coupled to a heat bath of fixed temperature in a manner which, under the quasiergodic hypothesis, gives canonical averages of static properties. Since the forces

*Permanent address: Institute of Theoretical Physics, Technical University of Berlin, Hardenbergstrasse 36, D-10623 Berlin, Germany.

in the Nosé method are momentum dependent, a propagation algorithm is necessary that calculates accurately both the configurations and the momenta. For this purpose a fourth-order Gear predictor-corrector method [33,34] was used to propagate the $(6N+2)$-dimensional system of first-order ordinary differential equations. A time step of 3×10^{-15} s was required to conserve the energy of the total system, i.e., of the cluster and the heat bath, from step to step to at least five significant digits as well as to prevent it from drifting over time. We fixed N and chose free-boundary conditions so that the atoms may evaporate from the clusters. In the temperature range relevant for phase changes evaporations occurred rarely, however.

To keep the cluster from starting on a high-symmetry manifold in configuration space, thus possibly destroying the assumed ergodicity, we distorted the icosahedral ground state, the global minimum-energy structure for magic-number sizes of homogeneous clusters with pairwise, centrosymmetric forces, by randomly displacing the coordinates of each atom. The initial momentum was chosen to be zero to avoid the complication of nonzero angular momentum. Before the averaging process began, fluctuations of the bath variable were damped by frequent zeroing of the corresponding momentum during the course of a preliminary run of 8×10^2 time steps. The cluster was then equilibrated for 5×10^3 time steps before the averaging process was initiated. We additionally quenched the cluster periodically during the runs, locating the potential surface minima with the conjugate gradient [35] minimization technique. In this method the potential energy of the system is minimized along $3N-6$ mutually orthogonal directions, so that the minimization performed along each such direction is independent of all the others.

As suitable diagnostics for the phase-change behavior we calculated the short-time mean potential energy, the short-time mean internal (kinetic plus potential) energy, the radial distribution of atoms, the individual, shell-by-shell mean-square displacements for each phase, and the dependence of the vibrational entropy on the potential energy for a characteristic sample of quenched states.

B. Results

What we call "phase" in the context of small clusters must be understood to be a form that exhibits the equilibrium properties we associate with bulk phases, at least for time intervals long enough to permit spectroscopic probing. Phases in the sense we use the term are, however, only the small-system analogs of bulk phases, not identical to bulk phases, and in particular are in dynamic equilibrium. The coexistence of two phases of a cluster thus normally means that the cluster in its history passes among the coexisting phases, spending relatively long times in each but visiting them all for time intervals whose ratios of average dwell times are given by the exponentials of the free-energy differences between pairs of phases, in units of kT.

The method of recognizing dynamic phase coexistence in isothermal MD is to compute short-time averages of the cluster's potential or total energy over a few of its breathing periods; when plotted against time, these distributions separate into distinct bands, each of which is easily distinguished by eye if the cluster stays in a particular potential-energy region for times long relative to the characteristic breathing period of the cluster. Rather than the potential energy, we averaged over the total (or internal) energy $E_{\rm tot}$ of the cluster to generate Figs. 1 and 2. Since the fluctuations of the kinetic temperature occur on the same time scale as the characteristic breathing periods of the potential energy, the picture of the short-time averages as a function of time remains unchanged; with increasing T, one merely observes a shift to higher values of the kinetic energy $E_{\rm kin}=kT/[2(3N-6)]$, where T is the temperature of the heat bath. Figure 1 shows the short time mean total energy $\langle E_{\rm tot}\rangle_\tau$ for different temperatures of Ar_{55}, where an averaging interval of $\tau=1800$ time steps has been used. At $T=30$ K, below the temperature of the onset of phase coexistence, we see a unimodal distribution of energies that correspond to vibrational states around the icosahedral ground state, whose structure is shown in Fig. 3(a). At 33 K we observe a splitting of the total energy into two distinct bands. A typical structure of clusters with total energies in the upper band is shown in Fig. 3(b): an atom has popped out of the surface and occupies the adjacent outer shell (a "floater"), leaving behind a vacancy in the surface. For $T=35$ K two additional bands appear [Fig. 1(c) and 1(d)]: one very close to the upper band of Fig. 1(b), representing a two-floater state [barely visible in Fig. 1(c) but clearly observable in Fig. 1(d)] and a wider one at much higher energies. The latter represents clusters with an amorphous structure which we denote "homogeneously melted" (HM) as opposed to the structures in the two lower energy bands with floater-vacancy pairs and a solid core, which we call "surface melted" (SM). The justification for these names will become clear in the following discussion. For slightly higher temperatures the SM bands disappear and only the band corresponding to energies of the HM phase remains.

Figure 2 shows the caloric curve of Ar_{55} obtained from isothermal MD by averaging separately over the potential-energy values corresponding to the total-energy regions I, II, and III shown in Figs. 1(c) and 1(d). We find three coexistence regions: between 33 and 34 K the solid and SM phases (dark squares and open circles, respectively) coexist, in the range between 35 and 38 K we find a threefold coexistence with the additional HM phase (open triangles). Somewhere between 38 and 39 K the solid phase vanishes and a twofold coexistence remains until only the HM phase remains for temperatures higher than approximately 39 or 40 K. We can distinguish four characteristic temperatures for the Ar_{55} freezing-melting transition. They are, in ascending order, $T_{\rm SF}$ and $T_{\rm CF}$ denoting the lower limits of the existence range of a liquid surface and liquid core, respectively, and therefore defined as the respective freezing-limit temperatures, and $T_{\rm SM}$ and $T_{\rm CM}$ representing the corresponding upper limits, the melting limits. The latter indicate the melting temperatures of surface and core, respectively. The limits found for the coexistence ranges in Fig. 2 are

only very crude estimates, since simulations of an order of magnitude longer in time would be necessary to give reasonably accurate limits of stability, especially to find the low-temperature limits T_{SF} and T_{CF}. Far longer times would be required to give reliable frequency distributions for occupancy of the phases, i.e., to produce statistically based equilibrium constants.

Figure 4 shows the short-time mean total energy for Ar_{147} at 38 K. Again we find several bands, the lowest one corresponding to the icosahedral ground state and

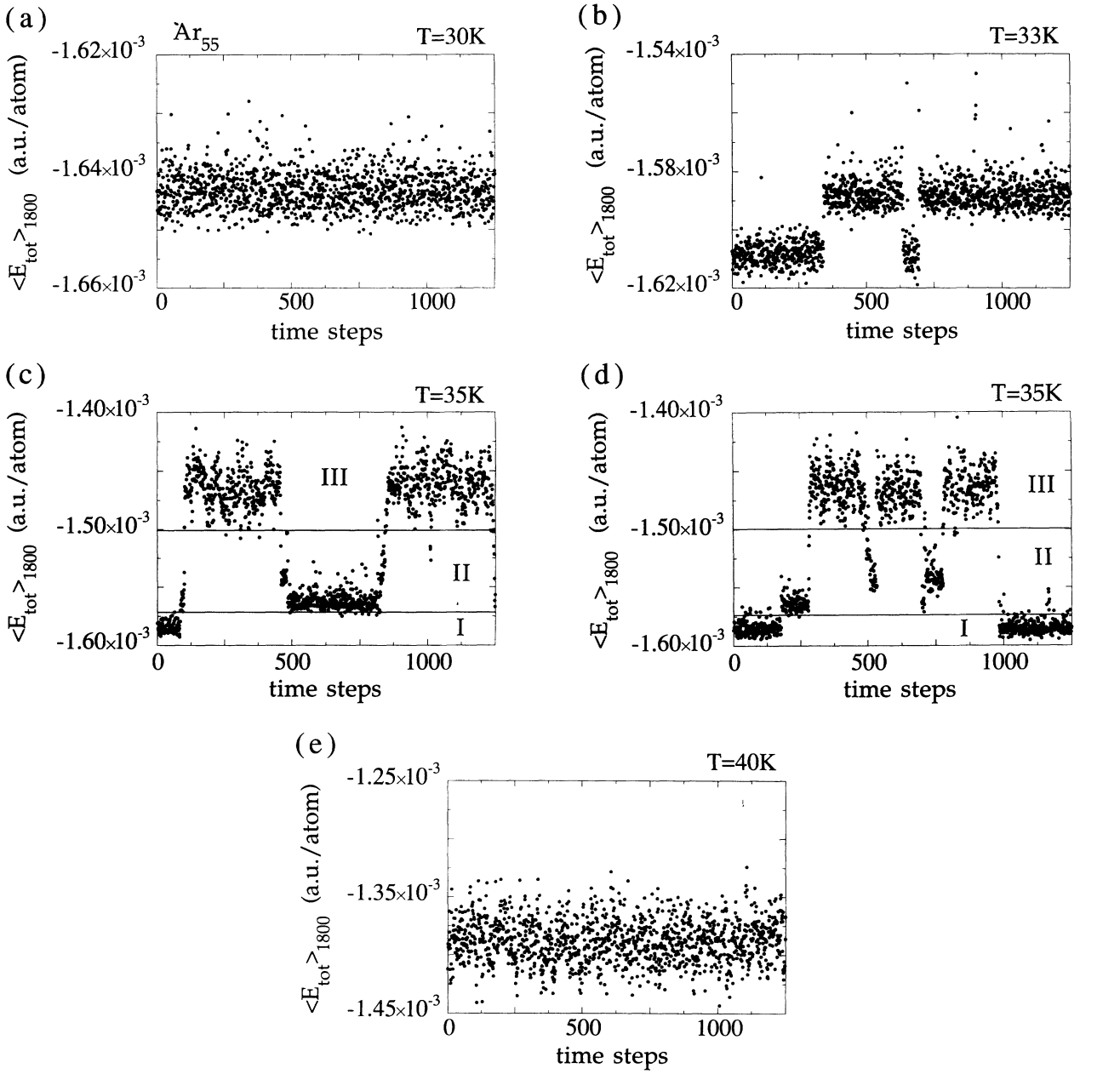

FIG. 1. The short-time-averaged internal energy $\langle E_{tot} \rangle_\tau$ for different temperatures of Ar_{55}. Each point represents an average over $\tau = 1800$ time steps of 3×10^{-15} s each. (a) At 30 K, before the onset of melting, the energy remains in one band representing a cluster whose energy is fluctuating around a mean value due to vibrational motion around the icosahedral ground state. (b) When the temperature is increased to 33 K an additional band of higher internal energy comes into play corresponding to a cluster with a solid core and one floater: the cluster can move back and forth between the two phases. It does this only occasionally, however, a given phase persisting for periods of time very long relative to the characteristic vibrational period. (c) and (d) At 35 K we find as additional phases of a dynamical coexistence a surface melted phase with two floaters and a homogeneously melted phase, in which the core and the surface of the cluster show liquidlike behavior. The solid lines in (c) and (d) correspond to the energy limits used in the simulations to distinguish between energy regions of the different phases, I denoting the solid phase, II the surface-melted phase, and III the homogeneously melted phase. (e) At 40 K the coexistence vanishes and only the homogeneously melted band persists.

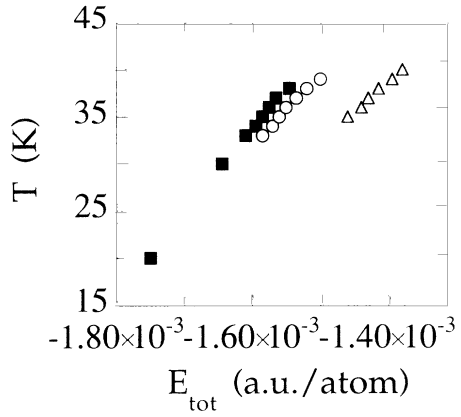

FIG. 2. Caloric curves of the solid (solid squares), surface melted (open circles), and homogeneously melted (open triangles) phases in Ar_{55} derived from the isothermal MD simulations.

the next two to surface melted states containing one, two, and three floaters, respectively. Our MD simulations of Ar_{147} also show dynamic coexistence of surface melted phases and the homogeneously melted phase. In order to find coexistence of S, SM, and HM phases in one run, however, simulations much longer in time than those we could perform are necessary.

To speak about different thermodynamic phases only makes sense, however, if the dynamics of the system allows it to spend long enough time intervals in each form to develop equilibrium properties characteristic of that form. To verify that the short-time averages presented in Figs. 1 and 4 are not artifacts of the length of the averaging interval τ (resulting, e.g., from a peak in the frequency spectrum of the energy close to $2\pi/\tau$) and to investigate the system's relevant time scales, we have calculated $\langle E_{\rm tot} \rangle_\tau$ for Ar_{55} at 35 K using three different averaging intervals $\tau = 1.8\times10^2$ time steps [Fig. 5(a)], 1.8×10^3 [Fig. 5(b)], and 1.8×10^4 [Fig. 5(c)]. For $\tau = 1.8\times10^2$ distinct energy bands can already be recognized although the fluctuations of the energy within each band are of the order of the energy shifts between the bands. For $\tau = 1.8\times10^3$ and 1.8×10^4 all the bands persist and no mixing can be found. From Fig. 5(c) the minimum duration of stay in a single phase can be estimated to be of the order of 6×10^2 breathing periods of 3×10^2 time steps each, assessing the average period of vibrational motion

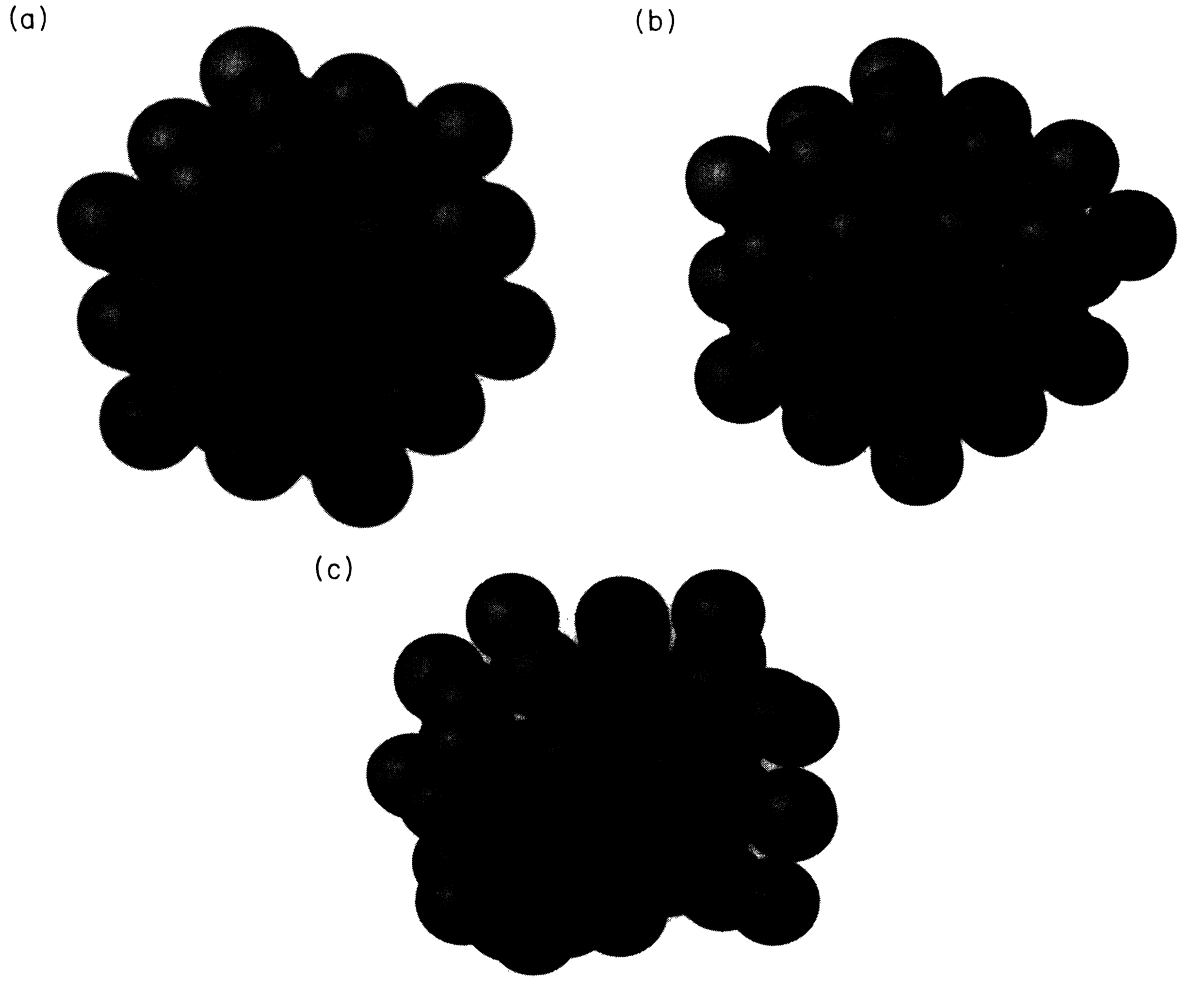

FIG. 3. Representative (quenched) structures of the coexisting phases in Ar_{55}: (a) solid icosahedral, $\phi = -5.292\times10^{-2}$ eV/atom, (b) surface melted with one floater, $\phi = -5.242\times10^{-2}$ eV/atom, and (c) homogeneously melted, $\phi = -5.027\times10^{-2}$ eV/atom. The core atoms and the floaters are represented by dark spheres, the outer shell atoms by light ones.

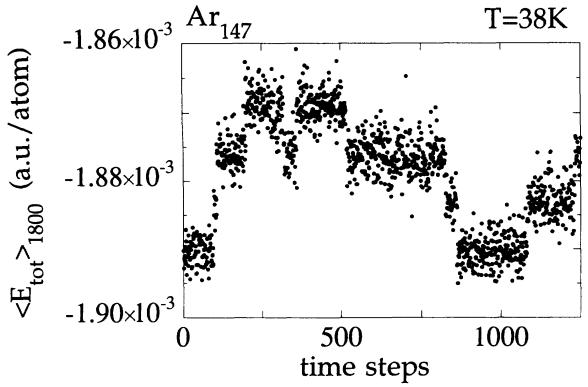

FIG. 4. The short-time-averaged internal energy $\langle E_{\rm tot}\rangle_\tau$, $\tau=1800$ time steps, for Ar_{147} at $T=38$ K. The dynamical coexistence between the solid phase (lower band) and three surface melted phases with one, two, and three floaters, respectively, is shown.

by inspecting individual trajectories.

To learn more about the properties of the different phases we have calculated the probability distribution $P(d)$ that a particle be the distance d from the center of mass (Fig. 6). The statistical ensemble for each phase was determined to consist of those points of the trajectory lying within a designated range of total energy. For Ar_{55} at 35 K these energy ranges are shown in Figs. 1(c) and 1(d). Region I corresponds to the solid phase, region II to the SM phase, and region III to the HM phase. Due to the cluster's energy fluctuations across these artificially set limits, the ensemble averages do not represent pure phases and contain mixing contributions between different phases. The statistical weight for each phase is by far highest within its own region; consequently, they give us a good qualitative picture of the properties that distinguish the phases. The average over region I (thin solid line) exhibits the pronounced shell-like structure of the Mackay icosahedra. There is no intershell motion due to the vanishing of $P(d)$ between the shells. In region II (heavy dashed line) the shell-like structure persists, although the peaks flatten slightly. There is, however, an additional nonzero contribution for values of d greater than that of the outermost shell. It arises from floaters. In region III particle exchange occurs between all shells, the shell-like structure becomes less pronounced, and the cluster looks amorphous in snapshots. The distribution can no longer be described by a superposition of Gaussian functions, and the intershell interactions and exchanges become relevant.

Figure 7 shows the averaged shell-by-shell mean-square displacements (MSDs) of Ar_{55} in the threefold phase coexistence region. The MSD for shell k with particle number N_k is given by

$$\langle \mathbf{r}^2(t)\rangle_k=\frac{1}{N_k}\sum_{\text{shell } k}\langle[\mathbf{r}_i(t)-\mathbf{r}_i(0)]^2\rangle\ , \tag{2}$$

where the average is over many independent time origins, in our case 1×10^3. Again we differentiated between the phases, making the classification into each phase on the basis of the energy region of the initial point. Since the ratio of sampling time of the MSD and the minimum duration of the system's residence in one phase is short ($<\frac{3}{180}\ll1$), the error in the MSD due to crossovers between phases during the calculation of one MSD sample is negligible. From the slopes of the shell-by-shell MSD the diffusion coefficients for each shell and phase can be calculated:

$$D_k=\frac{1}{6}\frac{d\langle \mathbf{r}^2(t)\rangle_k}{dt}\ . \tag{3}$$

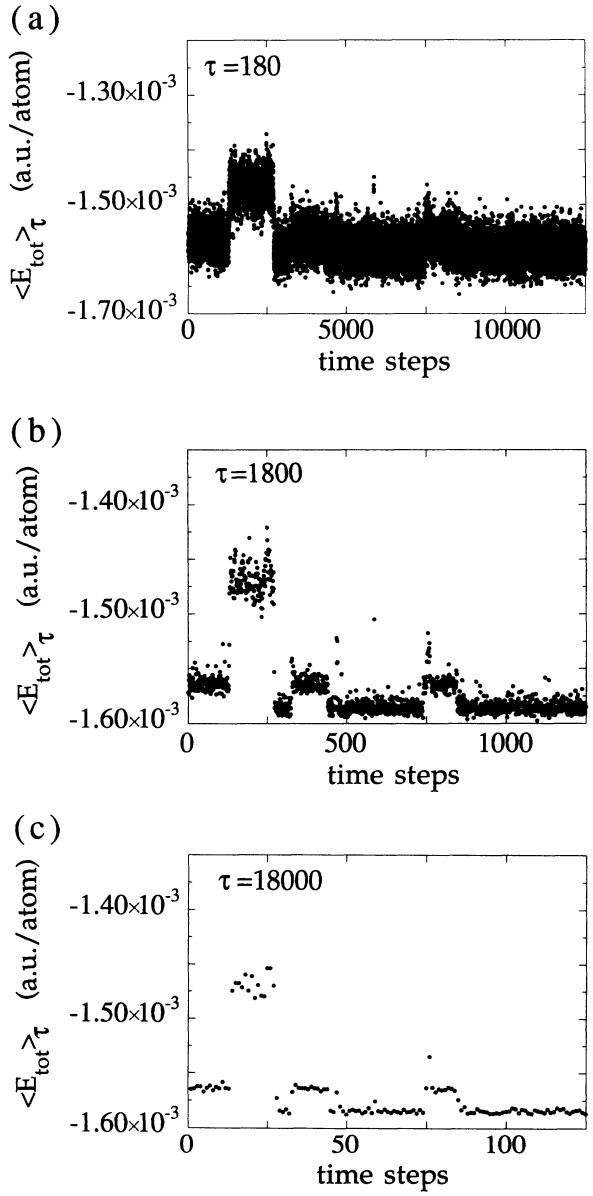

FIG. 5. The short-time-averaged internal energy $\langle E_{\rm tot}\rangle_\tau$ for Ar_{55} at $T=35$ K for different averaging times τ: each point corresponds to an average (a) over 1.8×10^2 iteration time steps, (b) over 1.8×10^3, and (c) over 1.8×10^4. The separation of phases in time is discernible in all three cases.

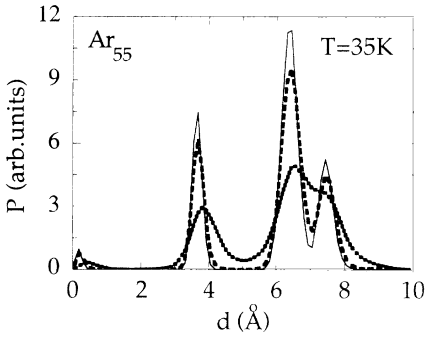

FIG. 6. Probability distributions of the distance d from the center of mass averaged over the regions in Fig. 1 separately for one constant-temperature MD run of Ar_{55} at $T=35$ K: the average over region I (thin solid line) exhibits the pronounced shell-like structure of Mackay icosahedra. There is no intershell motion due to the vanishing distribution $P(d)$ between the shells. In region II (heavy dashed line) the shell-like structure persists, although the peaks flatten slightly. There is, however, an additional nonzero contribution for values of d greater than that of the outermost shell stemming from floaters. In region III particle exchange between all shells occurs and the shell-like structure becomes amorphous.

For Ar_{55} at 35 K the diffusion coefficients computed from Fig. 7 are given in Table I. From the solid to the HM phase the diffusion constant of each shell in Ar_{55} increases by a factor of at least 20. The stiff localized motion of the particles in the solid transforms into delocalized diffusive motion characteristic of a liquid. Whereas the diffusion constant D_4 of the outer shell in the HM phase hardly differs from the corresponding constant D_1 of the center particle, D_4 has 4.5 times the value of D_1 in the SM phase. The absolute value of D_4 there, however still lies an order of magnitude below the values of the HM case. We can conclude that the floater-vacancy pairs exhibit diffusive motion, but that their motion is more restricted than any particle motion in the HM case.

As a further diagnostic tool to distinguish between the different phases we have computed the vibrational entropy $\sigma_{\rm vib}^{(h)}$ in the harmonic approximation for a sample of quenched states along the trajectory and identified their structures. The potential-energy hypersurface $\phi(\mathbf{r}_1,\mathbf{r}_2,\ldots,\mathbf{r}_N)$ can be approximated by a harmonic potential in the vicinity of its local minima, which we find by quenching, and the vibrational eigenfrequencies ω_i, $i=1,N$ can be computed from the Hessian matrix $(\partial^2\phi/\partial\mathbf{r}_i\partial\mathbf{r}_j)_{i,j}$. The vibrational entropy $\sigma_{\rm vib}^{(h)}$ is then given by

$$\sigma_{\rm vib}^{(h)}=k\sum_j \ln(\hbar\beta\omega_j)\ . \tag{4}$$

Figure 8 shows the harmonic vibrational entropy (normalized to the ground state) in terms of the potential energy ϕ for a sample of quenched states of Ar_{55}. The structure of each state was determined by computer visualization. We see an almost linear rise in the entropy for states with a solid core and m_f floaters, $m_f=0,1,2$, and a saturation at the three-floater state. The harmonic approximation supposes that the system stays near the local minimum of the potential-energy surface. At the temperatures in the range of surface melting and above, the floaters are not only able to go well above the harmonic regions of their potentials, but they go high enough to cross saddles fairly easily. From the diffusion coefficient D_4 in region II (cf. Table I) and the average vibrational period of floater motion, which was obtained from inspecting individual trajectories during the simulations and was found to lie around 3×10^2 time steps, the dwell time of a floater in each potential well can be estimated to be of the order of 50 breathing periods, so that floaters change wells fairly often during the life span of the SM phase. Hence $\sigma_{\rm vib}^{(h)}$ gives only a lower bound for the actual vibrational entropy. An upper bound can be obtained

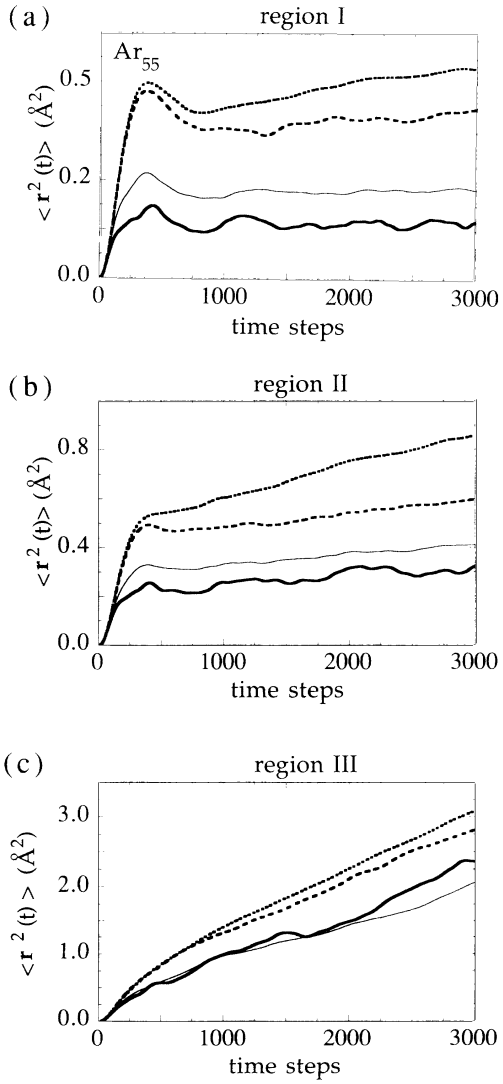

FIG. 7. Shell-by-shell mean-square displacements of Ar_{55} at $T=35$ K for each of the energetic regions I (a), II (b), and III (c), respectively. From the center outwards, the shells are represented by thick solid, thin solid, thin dotted, and heavy dotted lines, respectively.

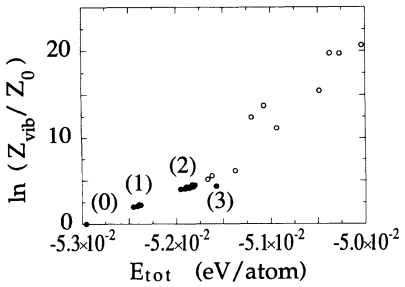

FIG. 8. The normalized vibrational entropy of quenched states of Ar_{55} as a function of their potential energy obtained from a harmonic approximation. The solid circles are states with a solid core and zero, one, two, or three floaters, respectively. The open circles represent clusters with an amorphous core and surface. For low floater numbers the entropy increases linearly and saturates for the three floater state, where the higher-energy homogeneously melted states begin to be advantageous entropically.

from a free-volume model without floater-floater interactions (especially excluded volume, i.e., strong repulsive interactions). This would only be expected to show saturation close to the half-empty shell levels. The simulations indicate an intermediate situation, so that the actual saturation is likely to occur at floater numbers a little above 3. Supposing that the actual entropy is not much larger than $\sigma_{vib}^{(h)}$, Fig. 8 shows HM states to be advantageous to SM states with floater numbers larger than 2. The saturation of the entropy for small floater densities $\rho_f \equiv m_f/N_s$, where N_s is the number of particles on the cluster surface, suggested by $\sigma_{vib}^{(h)}$, together with the strong rise in the entropy of the HM phase with increasing ϕ, might explain why the maximum number of floaters observed in computer simulations [17] is much smaller than the number of outer-layer atoms.

The multiple phase coexistence reported in this study for isothermal MD simulations of Ar_{55} and Ar_{147} with free-boundary conditions has also been observed in Monte Carlo (MC) simulations of Ar_{55}, the cluster having been placed within a hard constraining sphere. Nauchitel and Pertsin [29] report that the result of their MC run was "extremely 'unstable' in the [surface melted] region in the sense that all three phase states of the cluster could be here observed depending on the starting configuration and the sequence of random numbers used to generate the MC chain. Moreover, there sometimes occurred 'jumps' from one phase state to another within a single MC chain." The theoretical framework of dynamic phase coexistence in small systems was not yet developed when this was written. Consequently Nauchitel and Pertsin still thought of the melting-freezing transition of small Lennard-Jones systems in bulk terms, and considered the surface melted state in clusters the small system analog of the "two phase" state in bulk systems, in which solid and liquid phases are present together in one physical system. They did not recognize that they were observing dynamical coexistence of three phases. Instead, they considered "the observed instability to mask the true behavior of the internal energy-vs-temperature curve in the vicinity of the melting temperature," which they thought of as having the shape of an integrated λ peak.

TABLE I. Typical diffusion coefficients D_k for Ar_{55} at 35 K. The units used are 10^5 cm^2 s^{-1}.

Shell	Region I	Region II	Region III
1	$<5.0\times10^{-5}$	7.1×10^{-4}	1.3×10^{-2}
2	6.2×10^{-5}	8.0×10^{-4}	7.0×10^{-2}
3	4.3×10^{-4}	1.0×10^{-3}	1.4×10^{-2}
4	8.6×10^{-4}	3.1×10^{-3}	1.5×10^{-2}

Using a Metropolis sampling algorithm, Labastie and Whetten [30], on the other hand, report a solid-liquid coexistence from their MC simulations, but do not find the SM phase. The fact that surface melting did not contribute noticeably to the statistical sample they gathered might stem from the properties of the sampling algorithm of the Metropolis MC method and of the density of locally stable configurational states Ω in the SM region. From data gathered during the isothermal MD simulations, Ω can be computed by a technique presented in Ref. [18]. The result for Ar_{55} is that the values of Ω are nearly degenerate in ϕ for each of the two SM phases: the absolute values of Ω for the two SM forms, with one and two floaters, respectively, are 2.7×10^{17} and 1.3×10^{19} as compared to the maximum value of 6.2×10^{27} in the HM phase [36]. If the initial configuration of a Metropolis MC run does not lie within the energetically thin SM shell, the Markov chain used for the sampling might well find the solid-liquid, i.e., the solid-HM, transition without ever finding the SM states, so they do not contribute to the averaging process. This is opposed to the situation in isothermal MD runs, in which the dynamical equations virtually require the system to pass through the SM phases when changing from solid to homogeneous liquid.

In Sec. II B we presented the results of isothermal MD simulations showing a multiple phase coexistence in the melting-freezing transition of rare-gas clusters. In Sec. III we derive a simple statistical-mechanical model with which we can investigate the conditions for such behavior.

III. SIMPLE MELTING THEORY

A. Model

The conception of the model presented here is the formal separation of the clusters's statistical-mechanical properties into three subsystems, the cluster core, the surface layer, and the floaters, respectively. We suppose each cluster has N atoms, which we write as $N=N_M(n)+\alpha$ in the proximity of the Mackay numbers $N_M(n)=(2n+1)[1+5/3n(n+1)]$ with index n [37], where α can be either positive or negative. If α is small compared with $|N_M(n)-N_M(n\pm1)|$ then these categories are well defined. In the ground state the core and surface contain $N_c \equiv N_M(n-1)$ and $N_s \equiv N_n - \alpha\Theta(-\alpha)$, particles, respectively, where $N_n \equiv N_M(n)-N_M(n-1)$ and Θ is the Heaviside function. In this case there are also

$\alpha\Theta(\alpha)$ floaters. For a negative α approaching $-N_{n-1}/2$ or a positive α approaching $N_{n+1}/2$, the notions of surface layers and floaters as distinct categories lose their meaning.

The starting point for the investigation of the cluster's melting behavior is the partition function Z_N in (5) which we express in terms of the number of core or internal defects m_c, of surface defects m_s, and of floaters m_f:

$$Z_N = VZ_{\text{vib}}^{(0)} \exp(-\beta E^{(0)}) \sum_{m_c=0}^{N_d} \sum_{m_s=-\alpha\Theta(-\alpha)}^{N_n/2} \sum_{m_f=\alpha\Theta(\alpha)}^{N_{n+1}/2} \tilde{Z}_c(m_c)\tilde{Z}_s(m_s)\tilde{Z}_f(m_f)\tilde{Z}_{\text{int}}(m_c,m_s,m_f) , \quad (5)$$

with the summation indices restricted by the condition that $m_s - m_f + \alpha = 0$. The numbers of floaters and vacancies m_f and m_s cannot vary independently, but are related to each other by $m_s - m_f + \alpha = 0$, since we allow no particles to evaporate from the outermost layer. It is most appropriate to view the independent variable as m_s if $\alpha \geq 0$ and m_f otherwise. In (5) $\beta \equiv 1/kT$, V is the volume, $E^{(0)}$ and $Z_{\text{vib}}^{(0)}$ denote the potential energy and the vibrational partition function of the ground state, respectively, and N_d is the number of possible defect sites in the core. In the absence of interactions the normalized part of Z_N factors into contributions $\tilde{Z}_i$, $i = c,s,f$, corresponding to each subsystem. The factor $\tilde{Z}_{\text{int}}$ then takes into account entropic and energetic interactions between the subsystems.

For the core we follow Wales and Berry [4], who generalized a model Stillinger and Weber [38] formulated for the melting-freezing process on the basis of their computer simulations of argon clusters in a body-centered-cubic ground state lattice. Their formulation, which is similar to that used in the hole theory of dense fluids [39], was suggested by the concept of an inherent lattice arising naturally from Stillinger and Weber's quenched simulations. Using a quasiparticle formulation and working in the limit of a low density of defects, a simple consideration of the allowed permutations and a mean-field assumption for the energy led them to an expression for the partition function

$$\tilde{Z}_c = B(N_d, m_c) \frac{1}{\Lambda^{3m_c}} \left[\frac{V_c}{N_d} \right]^{m_c} e^{-\beta \Delta E^{(c)}} , \quad (6)$$

where B denotes the binomial function, $\Delta E^{(c)} \equiv E^{(c)} - E^{(0)}$ is the energy deviation of the core from the ground state, $\Lambda = (h^2/2\pi MkT)^{3/2}$, M is the quasiparticle mass, and V_c is the core volume. Whereas an energy expansion in terms of the number density of particles is not expected to be useful for a condensed system, an expansion in terms of the number density of defects $\rho_c \equiv m_c/N_d$ is appropriate if the system of quasiparticles is reasonably dilute. Expanding $e^{(c)} \equiv \Delta E^{(c)}/N_d$ we obtain

$$e^{(c)} = \sum_{k=0}^{\infty} \frac{1}{k!} [a_k^{(c)} + b_k^{(c)}(\beta)] \rho_c^k . \quad (7)$$

More specific models, such as Stillinger and Weber's [38], where the quasiparticles are actually composed of two particles and particles are allowed to appear together in the same cell, merely lead to quantitative changes of the melting properties; the fact remains that $\beta(\rho_c)$ has turning points only in the case of mutually attracting quasiparticles; this will be shown below.

$\tilde{Z}_s$ and $\tilde{Z}_f$ describe the deviation of the partition function from the ground-state value due to the effect of vacancies in the surface layer and of floaters, respectively. They are defined as

$$\tilde{Z}_i = \tilde{Z}_{\text{vib}}^{(i)}(m_i)\tilde{Z}_{\pi}^{(i)}(m_i) \exp[\mp \beta \Delta E^{(i)}(m_i)] , \quad i = s,f . \quad (8)$$

Here $\tilde{Z}_{\text{vib}}^{(i)}$ and $\tilde{Z}_{\pi}^{(i)}$ are the vibrational and permutational partition functions, respectively, and $\Delta E^{(i)} \equiv E^{(i)} - E^{(0)}$, $i = s,f$, are the energies of the surface and floater systems, respectively, normalized to the ground state. Counting the allowed permutations for the surface vacancies, one obtains $\tilde{Z}_{\pi}^{(s)} = B(N_s, m_s)$. An evaluation of $\tilde{Z}_{\pi}^{(f)}$ is more difficult, however, and resembles the problem of "communal entropy" [39], since the floaters can perform diffusive motion throughout the outer layer. The simulations show that the floaters vibrate around one site for many periods and only about once every 50 periods pass from one minimum to another and less frequently exchange with surface atoms. In this case the floaters' permutational partition function can be approximated by $\tilde{Z}_{\pi}^{(f)} = B[N_{n+1} - cm_s, m_f]$, in which we take into account the fact that floater sites adjacent to surface vacancies, of which there are assumed to be c for each vacancy, are excluded since the resulting vacancy-floater sites would be unstable. Prior to the onset of homogeneous melting $m_s \ll N_{n+1}/c$ holds, however, so that we obtain $\tilde{Z}_{\pi}^{(f)} = B[N_{n+1}, m_f] + O(m_f m_s)$. The energies $\Delta E^{(i)}$, $i = s,f$, can be defined analogously to (7) by the expansion of $e^{(i)} \equiv \Delta E^{(i)}/N_s$ in terms of the number densities of vacancies or floaters $\rho_i \equiv m_i/N_s$.

Interactions between different subsystems are incorporated into $\tilde{Z}_{\text{int}} \equiv \exp(-\beta N_s e_{\text{int}})$, where e_{int} can be expanded in terms of ρ_i, $i = c,s,f$, again assuming sufficiently dilute subsystems:

$$e_{\text{int}} = \sum_{l,l'=1}^{\infty} \{ [a_{l,l'}^{(cs)} + b_{l,l'}^{(cs)}(\beta)] \rho_c^l \rho_s^{l'} + [a_{l,l'}^{(sf)} + b_{l,l'}^{(sf)}(\beta)] \rho_s^l \rho_f^{l'} + [a_{l,l'}^{(cf)} + b_{l,l'}^{(cf)}(\beta)] \rho_c^l \rho_f^{l'} \} . \quad (9)$$

B. Local extrema in the case of vanishing interlayer interaction

Explicitly neglecting fluctuations, we can replace the sums in Z_N by their dominant terms in a maximum term

approximation. These can be found for fixed, sufficiently large N by taking the natural logarithm, applying Stirling's approximation, and differentiating with regard to $\mathbf{m}\equiv^{T}(m_c,m_i)$, where we now denote the independent surface variable by m_i and the dependent one by m_j. In the case of vanishing interlayer interaction, which we investigate in this subsection, the differentiation can be conducted independently for the core and the surface-floater system, respectively.

Let us first calculate the extrema of $\tilde{Z}_c$. From (6) we obtain

$$\left[\frac{\partial \ln\tilde{Z}_c}{\partial m_c}\right]_{\beta} = -3\ln\Lambda + \ln\left[\frac{V_c}{N_d}\right] + \ln\left[\frac{N_d}{m_c}-1\right] - \beta N_d \frac{\partial e^{(c)}}{\partial m_c} . \tag{10}$$

The condition for this derivative to vanish and hence for an extremum $\bar{m}_c$ of the free energy is therefore

$$\beta = \frac{\ln(1/\rho_c - 1) + \ln(V_c/N_d) - 3\ln\Lambda}{\partial e^{(c)}/\partial \rho_c} , \tag{11}$$

where we are using $\rho_c \equiv \bar{m}_c/N_d$ instead of $\bar{m}_c$. Due to the theorem of implicit functions and the nature of the partition function, the turning points of $\beta(\bar{m}_c)$, defined by $d\beta/d\bar{m}_c = 0$, also solve

$$\left[\frac{\partial^2 \ln\tilde{Z}_c}{\partial m_c^2}\right]_{\beta, m_c=\bar{m}_c} = N_d[(\rho_c-1)\rho_c]^{-1} - \frac{1}{N_d}\beta\frac{\partial^2 e^{(c)}}{\partial \rho_c^2} = 0 . \tag{12}$$

Since the fractional number density of quasiparticles is less than one, we will only find turning points for β as a function of ρ_c if the second derivative $\partial^2 e^{(c)}/\partial\rho_c^2$ can be negative. This requires the terms in $a_2^{(c)}$, $b_2^{(c)}$, $a_3^{(c)}$, $b_3^{(c)}$, etc. to make a negative contribution to the second derivative of the energy. Interpreting the defect-defect interaction terms in $e^{(c)}$ proportional to ρ_c^2, ρ_c^3, etc. as two-body,

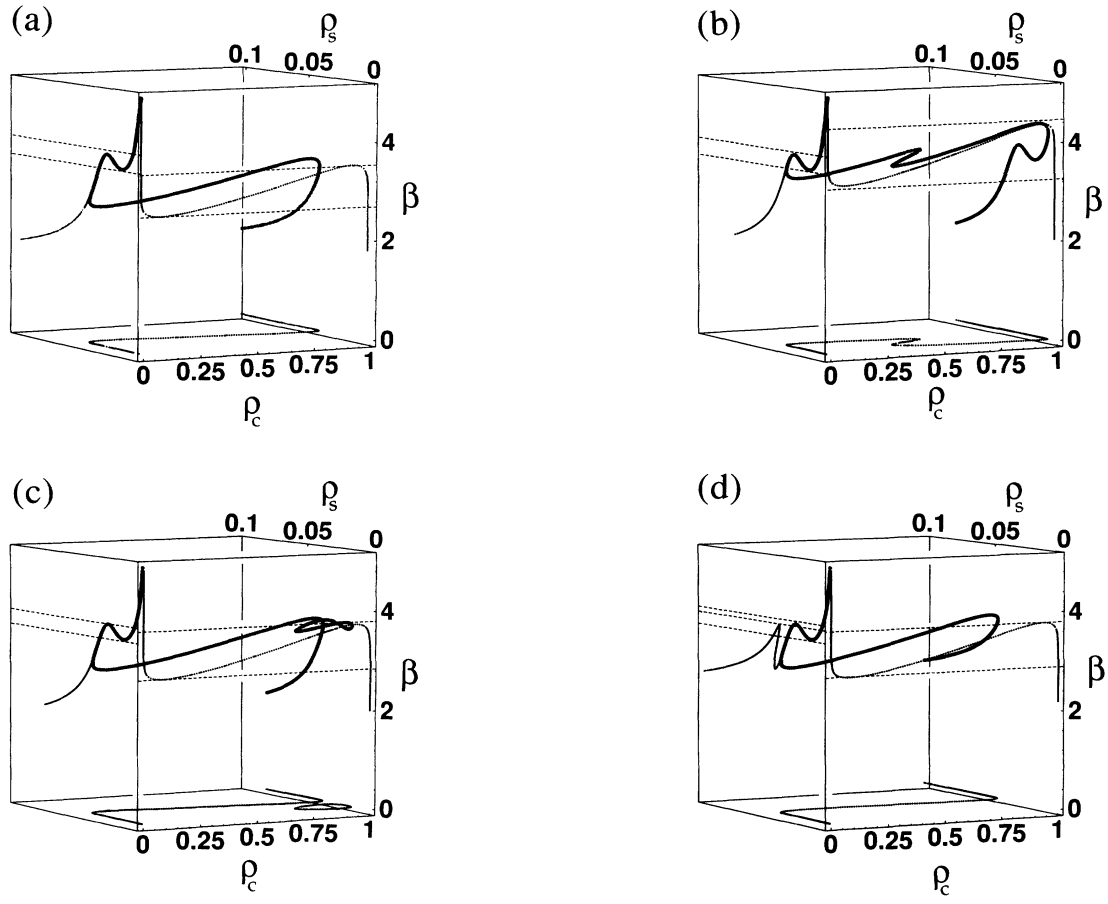

FIG. 9. The inverse temperature β as a function of the density of core defects ρ_c and surface vacancies ρ_s. (a)–(c) show the case of vanishing interlayer interaction $\xi_1,\xi_2=0$ for different overlaps of the coexistence regions $[\beta_{CM},\beta_{CF}]$ for the core and $[\beta_{SM},\beta_{SF}]$ for the surface. (d) is the same as (c) except for $\xi_2=-100$. For (c) and (d) we used parameters adequate for Ar_{55}. β_{SF} and β_{SM} are represented by dashed lines in the (β,ρ_s) basal plane, β_{CF} and β_{CM} by dashed lines in the (β,ρ_c) basal plane. In (d) β_{CF} has been extended to the (β,ρ_s) plane. The parameters we used are (a) $N_d=N_c$, $\Delta e_1^{(sf)}=2.287$, $\Delta e_2^{(sf)}=0.101$, $\gamma_1=5.428\times10^{-2}$, $\gamma_2=4.29\times10^{-2}$, $\gamma_3=2.0$, $\delta=2.8\times10^{-2}$, $e_1^{(c)}=7.69\times10^{-1}$, $e_2^{(c)}=-(2.31\times10^{-1}+3.85\times10^{-1}/\beta)$, and $\ln(V_c/N_d\Lambda^3)=23.5$. (b) Same as (a) except for $\ln(V_c/N_d\Lambda^3)=29.5$. (c) Same as (a) except for $\ln(V_c/N_d\Lambda^3)=25$.

three-body, and higher corrections, we see that turning points will occur if these interactions are energy lowering, i.e., if there are attractive forces between the quasiparticles.

The equation defining $\beta(\bar{m}_i)$ [$(i,j)=(s,f)$ for $\alpha \geq 0$ and vice versa otherwise] in the interactionless case is given by

$$\left[\frac{\partial \ln[\tilde{Z}_i(m_i)\tilde{Z}_j(m_i+|\alpha|)]}{\partial m_i}\right]_{\beta, m=\bar{m}} = 0 \ . \tag{13}$$

Again using Stirling's approximation we obtain from (8)

$$\left[\frac{\partial \ln[\tilde{Z}^{(i)}_{\text{vib}}(m_i)\tilde{Z}^{(j)}_{\text{vib}}(m_i+|\alpha|)]}{\partial m_i}\right]_{\beta, m=\bar{m}} + \ln\left[\frac{N_i}{\bar{m}_i}-1\right] + \ln\left[\frac{N_j}{\bar{m}_i+|\alpha|}-1\right] \mp \beta N_s \frac{\partial}{\partial m_i}[e^{(i)}(m_i)-e^{(j)}(m_i+|\alpha|)]_{\beta, m=\bar{m}} = 0 \ , \tag{14}$$

where the minus sign holds for $i=s$ and the plus sign for $i=f$ and $N_f \equiv N_{n+1}$ has been introduced. The first term in (14) can be expressed as the derivative of

$$\tilde{\sigma}_{\text{vib}}(m_i) \equiv \ln[\tilde{Z}^{(i)}_{\text{vib}}(m_i)\tilde{Z}^{(j)}_{\text{vib}}(m_i+|\alpha|)] = \ln\left[\frac{Z_{\text{vib}}(m_c=0, m_i, m_i+|\alpha|)}{Z^{(0)}_{\text{vib}}}\right] , \tag{15}$$

where Z_{vib} is the total vibrational partition function, since for $m_c=0$ the vibrational partition function of the core drops out due to the normalization. Note that (15) also holds if interlayer interactions are included. The explicit dependence of $\tilde{\sigma}_{\text{vib}}$ on m_i can be approximated from simulation data by calculating (4) for quenched states with a solid core and m_i floaters as well as for the ground state, and subsequent subtraction. For Ar_{55} (which is a magic number cluster, thus $\alpha=0$ and $i=s$ hold)

$$\tilde{\sigma}_{\text{vib}} = N_s\{\gamma_1 + \gamma_2 \arctan[\gamma_3(m_s - N_s\tilde{\rho})]\} \tag{16}$$

accommodates the simulation data with the fitting parameters γ_1, γ_2, γ_3, and $\tilde{\rho}$ (for parameter values, see Fig. 9). Again it must be pointed out that $\sigma^{(h)}_{\text{vib}}$ gives only a lower bound for the vibrational entropy, which we assume, however, to be represented well by $\sigma^{(h)}_{\text{vib}}$. With (14) and (16) we obtain $\beta(\bar{m}_s)$ for magic number clusters

$$\beta = \frac{N_s\gamma_2\gamma_3[1+(\gamma_3)^2(\bar{m}_2 - N_s\tilde{\rho})^2]^{-1} + \ln(N_s/\bar{m}_s - 1) + \ln(N_f/\bar{m}_s - 1)}{N_s \partial \Delta e^{(sf)}/\partial \bar{m}_s} \ , \tag{17}$$

where we have introduced $\Delta e^{(sf)} \equiv e^{(s)} - e^{(f)}$. The turning points of $\beta(\bar{m}_s)$ are given by

$$\left[\frac{\partial^2 \ln[\tilde{Z}_s(m_s)\tilde{Z}_f(m_s)]}{\partial m_s^2}\right]_{\beta, m_s=\bar{m}_s} = -\left\{\frac{2N_s\gamma_2(\gamma_3)^3(\bar{m}_s - N_s\tilde{\rho})}{[1+(\gamma_3)^2(\bar{m}_s - N\tilde{\rho})^2]^2} + \frac{N_s}{\bar{m}_s(N_s-\bar{m}_s)} + \frac{N_f}{\bar{m}_s(N_f-\bar{m}_s)}\right\} - \beta(\bar{m}_s)N_s\frac{\partial^2 \Delta e^{(sf)}}{\partial \bar{m}_s^2} = 0 \ , \tag{18}$$

where the dependence of β on $\bar{m}_s$ is given by (17). For reasons of simplicity let us now neglect all energy terms of cubic or higher order in $\bar{m}_s$. If $\tilde{\sigma}_{\text{vib}}$ were linear in $\bar{m}_s$, the first term in (18), being the second derivative of $\tilde{\sigma}_{\text{vib}}$ with respect to $\bar{m}_s$, would vanish. In this case, analogous to the core, a pair of turning points $\bar{m}^*_{1/2}$ would be found only if $\Delta e^{(sf)}_2 < 0$. Due to the properties of the second and third term in (18) $m^*_1 \leq N_s/2 \leq m^*_2$ would hold. Coexistence within the range of $\bar{m}_s \in [0, N_s/2]$, where the outer layer is still well defined, would not be possible. The nonlinearities of $\tilde{\sigma}_{\text{vib}}$, however, lead to a resonance-peaklike form of its second derivative $\tilde{\sigma}''_{\text{vib}} \equiv (\partial^2 \tilde{\sigma}_{\text{vib}}/\partial \bar{m}_s^2)_\beta$ around $N_s\tilde{\rho}$, making a second pair of turning points for negative values of $\Delta e^{(sf)}_2$ possible. They can even lead to a pair of turning points for positive $\Delta e^{(sf)}_2$ under a certain threshold if γ_2 is large enough. For $\tilde{\rho} \ll \frac{1}{2}$ the arctan shape of $\tilde{\sigma}_{\text{vib}}$ given in (16) is therefore sufficient to create the finite-system counterpart of a first-order melting-freezing transition of the surface in a range of $\bar{m}_s$ that is compatible with numerical experiments.

What are, however, the necessary conditions that $\tilde{\sigma}_{\text{vib}}$, the entropy of the surface vacancy-floater system, has to meet in order for a pair of turning points in the $\beta(\bar{m}_s)$ curve to appear with surface densities $\rho^*_{1/2} \equiv m^*_{1/2}/N_s \ll \frac{1}{2}$? Let us assume that σ''_{vib} has a single global maximum at $\tilde{m} \ll N_s/2$ and there are no other local extrema. Under sufficient conditions the curly bracket in (18) then has a single global maximum at a value of $\bar{m}_s$ much smaller than N_s, since the other terms are monotonically falling in $\bar{m}_s$. Negative values of $\Delta e^{(sf)}_2$ can then lead to four intersection points. Two of these points originate from the diverging behavior of the second term in (18) at $\bar{m}_s = 0$ and N_s and lie in the vicinity of the poles. The other two are created by σ''_{vib} and lie near $\tilde{m}$. Since $\tilde{\sigma}_{\text{vib}}$ is non-negative and $\tilde{\sigma}_{\text{vib}}(0)=0$ holds by definition (15), any function of $\bar{m}_s$ that increases for $\bar{m}_s < \tilde{m}$ and saturates at a value $\tilde{m}$ smaller than $N_s/2$ will have a single local maximum in its second derivative at $\tilde{m}$ and thus lead to the desired surface melting behavior. And indeed, the entropy values for a solid core and different values of $\bar{m}_s = \bar{m}_f$, gained from a harmonic approximation and shown in Fig. 8, exhibit a saturation

behavior at $\bar{m}=3<N_s/2=21$, suggesting a similar behavior for the actual vibrational entropy.

In the absence of interactions the classification of the extrema of the full system is easily determinable from that performed in each subsystem separately, since the eigenvalues of the Hessian $(\partial^2 \ln Z_N/\partial\bar{m}_i\partial\bar{m}_j)_\beta$, $i,j=c,s$, are given by $\lambda_c=(\partial^2\ln\tilde{Z}_c/\partial\bar{m}_c^2)_\beta$ and $\lambda_s=[\partial^2\ln(\tilde{Z}_s\tilde{Z}_f)/\partial\bar{m}_s^2]_\beta$. Analogously to $\beta(m_c)$ [4], descending branches of $\beta(\bar{m}_s)$ are local maxima of $\ln(\tilde{Z}_s\tilde{Z}_f)$ and thus have $\lambda_s<0$ if the derivative of the energy with respect to m_s is negative. Maxima of $\ln Z_N$ (i.e., minima of the free energy) therefore are those subsets of $(\bar{m}_c,\bar{m}_s)$, in which β is a decreasing function of both independent variables.

In order to find $\bar{m}_c(\beta)$ and $\bar{m}_s(\beta)$ the transcendental functions (11) and (17) can be inverted numerically. Instead, we do this graphically by plotting β as a function of ρ_c and ρ_s (alternatively to $\bar{m}_c$ and $\bar{m}_s$), in three dimensions. The interactionless case is shown in Figs. 9(a)–9(c) using three different sets of parameter values. In addition to the full space curve $\beta(\rho_c,\rho_s)$ (heavy line), its projections $\rho_s(\rho_c),\rho_c(\beta)$, and $\rho_s(\beta)$ onto the axis planes are visualized as thin lines.

Figure 9(a) exhibits separate coexistence regions for the core and the surface. For low temperatures (or high β) both the core and surface defect densities are close to zero. The cluster is solid. With increasing temperature (or decreasing β) the system reaches a value $\beta_{SF}\equiv 1/kT_{SF}$ at which a second extremum of $\ln Z_n$ appears at $\rho_s>0$. This temperature is the upper limit for the existence of a melted surface and can thus be seen as the "surface freezing" point. Since $\rho_c\approx 0$ still holds, the system changes from the solid phase (characterized by $\rho_c\approx 0,\rho_s\approx 0$) to coexisting solid and surface-melted ($\rho_c\approx 0,\rho_s\neq 0$) phases at β_{SF}. Lowering β further one reaches the temperature at which the extremum with $\rho_s\approx 0$ and, equivalent to it, the solid phase vanishes. This is the point of complete surface melting, represented by $\beta_{SM}\equiv 1/T_{SM}$. A further decrease of β leads to an analogous cycle for the core: as the surface remains melted, a second value of $\rho_c\approx 1$ maximizing $\ln Z$ appears at β_{CF}, the upper limit for the existence of melted core states and thus the core freezing point. Here the SM phase coexists with the HM phase in which both the core and the surface are melted ($\rho_c\approx 1,\rho_s\neq 0$). At $\beta_{CM}\equiv 1/T_{CM}$ the branch with $\rho_c\approx 0$ vanishes and the core melts, so only the HM phase remains. The (inverse) limit temperatures β_{SF} and β_{SM} are represented by dashed lines in the (β,ρ_s) basal plane in Figs. 9(a)–9(d), β_{CF} and β_{CM} by dashed lines in the (β,ρ_c) basal plane. In Fig. 9(d) β_{CF} has been extended to the (β,ρ_s) plane.

Figure 9(b) shows $\beta(\rho_c,\rho_s)$ in the case that the coexistence range of the surface is completely contained in that of the core. With increasing temperature or decreasing β we find the cluster in S, then in a region of coexistence of S and a phase with a melted core and a solid surface ["core melted" (CM), $\rho_c\approx 1,\rho_s\approx 0$], then in a coexistence zone of all four possible phases S, SM, CM, and HM, then in a coexistence of only SM and HM, and finally in a region of HM only.

Figure 9(c) displays $\beta(\rho_c,\rho_s)$ with core parameter values chosen in such a way that the core coexistence range $[\beta_{CM},\beta_{CF}]$ is that found in simulations of Ar_{55}. Here the overlap of the surface coexistence temperature band with that of the core is only partial. Again scanning through the temperature range starting at large β, we find S, a coexistence of S and SM, a fourfold coexistence of all possible states, again a twofold coexistence, this time of S and SM, and finally HM alone.

Figure 9(a)–9(c) display the temperature dependence of the phase behavior in the interactionless case for all possible scenarios of overlap of the coexistence regions. [Switching the coexistence regions in Fig. 9(c) merely leads to an exchange of S and C in the sequence of phases.] We conclude that in the absence of interactions between the core defects and the vacancy-floater pairs, the threefold coexistence of S, SM, and H we found in the simulations of Ar_{55} and infer from those of Ar_{147} cannot be explained in a mean-field model; either separate twofold phase coexistences or an intermediate fourfold coexistence persists. Additionally, it must be pointed out that the CM phase is an artifact of this omission: the fact that the core can melt independently of the state of the surface contradicts the dynamical behavior of the system governed by the underlying Newtonian equations of motion: they only allow a deviation of the core from the icosahedral energy-minimizing structure if the restraining forces acting from the surface are sufficiently small. This shortcoming is removed with the refinement of Sec. III C. One can, however, imagine a frozen surface around a molten core in the presence of unusual forces, such as those between water molecules, which permit solids to be less dense than the corresponding liquids.

C. Inclusion of interlayer interaction

In this section we calculate the extrema of $\ln Z_N$ assuming the interaction term $\tilde{Z}_{int}$ makes a nonvanishing contribution. As was the case for intralayer interactions, we restrict ourselves to terms of order smaller than cubic in the defect-floater densities, incorporating terms linear or quadratic with respect to ρ_c and ρ_i into $e^{(c)}$ and $e^{(i)}$ by renormalizing the coefficients of the energy expansion, so that

$$\begin{aligned} a_1^{(c)} &\to \tilde{a}_1^{(c)} = a_1^{(c)} \pm a_{1,1}^{(cj)} \frac{\alpha}{N_d} , \\ a_1^{(i)} &\to \tilde{a}_1^{(i)} = a_1^{(i)} \pm a_{1,1}^{(ij)} \frac{\alpha}{N_s} , \\ a_2^{(i)} &\to \tilde{a}_2^{(i)} = a_2^{(i)} \pm 2a_{1,1}^{(ij)} \end{aligned} \tag{19}$$

and equivalent substitution equations can be found for b. We find that e_{int} reduces to

$$e_{int}=[a_{1,1}^{(cs)}+a_{1,1}^{(cf)}+b_{1,1}^{(cs)}(\beta)+b_{1,1}^{(cf)}(\beta)]\rho_c\rho_i , \tag{20}$$

where we have dropped the tildes again.

From (5) we then obtain the defining equations for $\bar{m}_c$ and $\bar{m}_s$ in the presence of interlayer interactions

$$\left[\frac{\partial \ln Z_N}{\partial m_c}\right]_{\beta,m_c=\bar{m}_c}=\left[\frac{\partial \ln \tilde{Z}_c}{\partial m_c}\right]_{\beta,m_c=\bar{m}_c}-\frac{\beta\xi_1+\xi_2}{N_d}\rho_s=0\ , \tag{21}$$

$$\left[\frac{\partial \ln Z_N}{\partial m_s}\right]_{\beta,m_s=\bar{m}_s}=\frac{\partial}{\partial m_s}[\ln \tilde{Z}_s(m_s)\tilde{Z}_f(m_s)]_{\beta,m_s=\bar{m}_s}-\frac{\beta\xi_1+\xi_2}{N_s}\rho_c=0\ , \tag{22}$$

where we again restrict ourselves to the magic number case, and $\xi_1=N_s[a_{1,1}^{(cs)}+a_{1,1}^{(cf)}]$ and $\xi_2=N_s\beta[b_{1,1}^{(cs)}(\beta)+b_{1,1}^{(cf)}(\beta)]$ were introduced for simplicity. In the following we assume that the temperature-dependent contributions to the interlayer interaction energies $b_{1,1}^{(cs)}$ and $b_{1,1}^{(cf)}$, e.g., describing the coupling of core and surface defects by phonons, are linear in the temperature $T=1/k\beta$, making ξ_2 independent of β.

We obtain two equations for β corresponding to the derivatives of $\ln Z_N$ with regard to the two independent variables m_c and m_s:

$$\beta=\beta_c(\rho_c,\rho_s)\equiv\frac{\ln(1/\rho_c-1)+\ln[V_c/(N_d\Lambda^3)]-(\xi_2/N_d)\rho_s}{\partial e^{(c)}/\partial\rho_c+(\xi_1/N_d)\rho_s}\ , \tag{23}$$

$$\beta=\beta_s(\rho_c,\rho_s)\equiv\frac{N_s\gamma_2\gamma_3[1+(\gamma_3)^2N_s^2(\rho_s-\tilde{\rho})^2]^{-1}+\ln(1/\rho_s-1)+\ln[N_f/(\rho_sN_s)-1]-(\xi_2/N_s)\rho_c}{\partial\Delta e^{(sf)}/\partial\rho_s+(\xi_1/N_s)\rho_c}\ . \tag{24}$$

From the transcendental equation $\beta_c(\rho_c,\rho_s)-\beta_s(\rho_c,\rho_s)=0$ we find $\rho_s(\rho_c)$, which after insertion into (23) gives us $\beta(\rho_c)$ and, using $\rho_s(\rho_c)$, $\beta(\rho_s)$. Whether the extremum $\beta(\rho_c,\rho_s)$ is a maximum, a minimum, or a saddle of $\ln Z_N$ is determined by the trace Tr and determinant Det of the Hessian H:

$$H=\left[\frac{\partial^2 \ln Z_N}{\partial\bar{m}_i\partial\bar{m}_j}\right]_\beta=\delta_{ij}\left[\lambda_i+\frac{\beta\xi_1+\xi_2}{N_sN_d}\right]-\frac{\beta\xi_1+\xi_2}{N_sN_d}\ ,\quad i,j=c,s\ , \tag{25}$$

where λ_i are the eigenvalues in the case of vanishing interlayer interaction. For the respective cases, Tr $H<0$ and Det $H>0$, Tr $H>0$ and Det $H>0$, and Det $H\le 0$ hold. The inclusion of interlayer interaction only has a very small effect on the stability of the solution manifolds $\beta(\rho_c,\rho_s)$. Hence the criterion of the interactionless case, i.e., that β curves which are descending functions of both ρ_c and ρ_s are maxima of $\ln Z_N$, also holds here with good approximation.

Figure 9(c) shows $\beta(\rho_c,\rho_s)$ for $\xi_1,\xi_2=0$ and parameter values suitable to describe Ar_{55}. If a negative, i.e, energy-decreasing temperature-dependent interlayer interaction ξ_2, is assumed [Fig. 9(d)], the part of the curve in the CM regime that is not connected with the rest shrinks and finally vanishes. Figure 9(d) shows that a coexistence of S, SM, and HM takes place between β_{CF} and β_{SM}. For large β we find a coexistence of SM and S and, if $\beta>\beta_{SF}$, merely the solid phase. The condition $\beta_{CM}<\beta<\beta_{SM}$ yields a SM-HM coexistence, and for $\beta<\beta_{CM}$ we find only HM. In Fig. 10 $\rho_s(\rho_c)$ is compared for $\xi_1=-10$ [Fig. 10(a)], $\xi_1=0$ [Fig. 10(b)], and $\xi_1=10$ [Fig. 10(c)] and several values of ξ_2. One sees that the value of $\xi_2<0$ at which the core-melted state vanishes for $\xi_1=0$ increases if the energetic interaction is negative, i.e., the two-body forces between the core and surface quasiparticles are attractive. Comparing, e.g., the $\rho_s(\rho_c)$ curves for $\xi_2=0$ [heavy solid lines in Figs. 10(a)–10(c)], the CM phase that exists for an energy-increasing temperature-dependent interaction $\xi_1=10$ vanishes for $\xi_1=-10$.

From Figs. 9 and 10 we can therefore conclude that the multiphase coexistence of S, SM, and CM that we find in MD simulations of Ar_{55} and infer from those of Ar_{147} can only be explained within the framework of a mean-field model if the interactions between core defects and floater-vacancy pairs are sufficiently energy lowering, i.e., that these quasiparticles either attract each other or have a mode-softening effect on the phonon spectrum, or both. This inference is similar to that made by Wales and Berry [4]. Clusters whose interatomic forces lead to a net repulsion of these quasiparticles will not exhibit a melted surface, since this phase would imply the existence of the "dual" core-melted phase. Mechanical considerations, however, make the appearance of such a phase unlikely for clusters bound by simple, central forces. Such clusters are more likely to exhibit a transition to a nonwetted phase, in which a solid and a liquid region coexist "side by side" simultaneously, which is the case, for example, for $(KCl)_{32}$ [18]. Here the dual state, in which the role of the core and the surface are simply exchanged, also corresponds to a physically reasonable structure, namely, the nonwetted one itself.

IV. DISCUSSION

The phase coexistence behavior we find in Ar_{55} and Ar_{147} allows us to make some general remarks on the nature of the surface-melting transition. As opposed to earlier suggestions [17], it resembles more a finite system's counterpart of a normal, first-order transition, rounded by finite-size effects [40,41] than the small-system analog of a weak first-order transition. In the previous work, the necessity of a small latent heat was recognized but the formalism did not allow enough flexibility to reveal the two-minimum or multiple-minimum form of the free en-

ergy as a function of the order parameter, at constant temperature and pressure. The solid surface clearly does not lose its local stability at the same temperature the liquid surface gains it. This stems from the fact that the entropy of the surface seems to saturate for a very low density of surface vacancy-floater pairs and cannot be treated as linear in the number of floaters within the transition range. A direct statistical-mechanical derivation of this behavior from the interatomic forces remains to be performed, however. The "melted surface" apparently does not provide nuclei for homogeneous melting, thus permitting superheating.

From a mean-field theory we further find that clusters will only exhibit a melted surface if the two-body interaction forces between core defects and the quasiparticles of the surface, i.e., floater-vacancy pairs, are attractive. From the symmetry of the CM and SM phases in (ρ_s,ρ_c) space, which accompanies repulsive core-surface interactions, we conclude that clusters with interatomic forces leading to such properties of the quasiparticles will more likely exhibit nonwetted structures. From the model we derived in Sec. III we can compute conditions the material parameters of the cluster have to meet for the cluster to show multiple phase coexistence. This has been done in the Appendix.

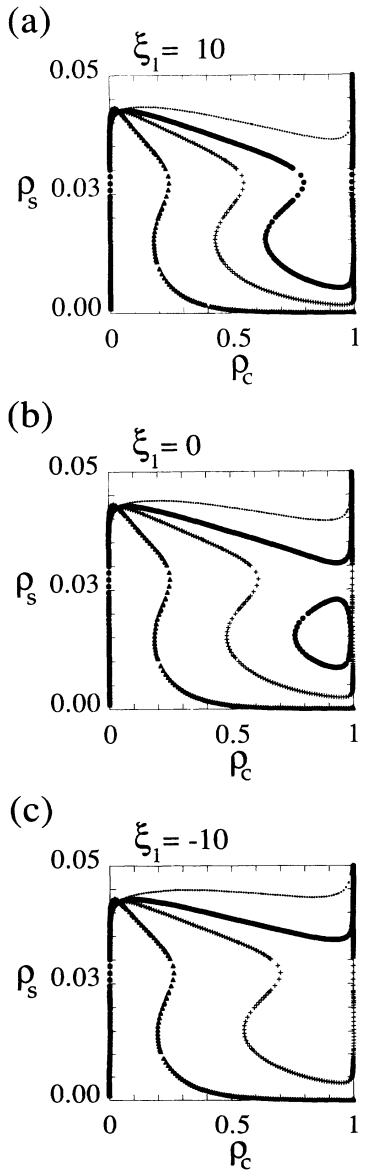

FIG. 10. The relation of surface to core density $\rho_s(\rho_c)$ for different values of the interlayer interactions ξ_1 and ξ_2: ξ_1 is given by (a) -10, (b) 0, and (c) 10; ξ_2 is 500 (solid triangles), 100 (crosses), 0 (heavy line), and -100 (thin line).

V. CONCLUSIONS

Isothermal MD simulations of Ar_{55} and, in a less complete way, of Ar_{147} clusters reveal a dynamic, multiple phase coexistence involving a solid, microcrystalline phase, a homogeneously melted phase, and phases exhibiting a solid core and a melted surface. A simple theory for the melting-freezing transition that incorporates heterogeneous phases shows that this behavior is possible if the core and surface both undergo finite-system analogs of first-order transitions with overlapping coexistence regions, and the mode-softening defects of the core exhibit an attractive interaction with the vacancy-floater pairs on the surface. Parameter dependences necessary for the existence of multiphase behavior are given.

ACKNOWLEDGMENTS

The authors would like to thank Dr. H.-P. Cheng and Dr. R. J. Hinde for many helpful discussions. We particularly appreciate the stimulating exchange of ideas with Dr. J. Rose and the use of his MD program. R.S.B. would like to acknowledge the stimulating comments of Dr. J. Cahn. The financial support of the German National Scholarship Foundation is gratefully acknowledged.

APPENDIX: CRITERIA FOR MULTIPLE-PHASE COEXISTENCE

In this appendix we will briefly give an algorithm with which criteria for the mean-field parameters of the model in Sec. III can be found so that multiple phases (i.e., more than two) coexist. The parameters N_d, $a_1^{(c)}$, $b_1^{(c)}$, etc., $\ln(V_c/N_d\Lambda^3)$ for the core and $a_1^{(s)}$, $b_1^{(s)}$, $a_1^{(f)}$, $b_1^{(f)}$, etc., γ_1, γ_2, γ_3, $\tilde{\delta}$ for the surface we will symbolically denote by $\mathbf{a}_c$ and $\mathbf{a}_s$, respectively. The condition for multiple phase coexistence (MPC) is then given by

$$\beta_{\mathrm{SM}}(\mathbf{a}_c,\mathbf{a}_s) \leq \beta_{\mathrm{CF}}(\mathbf{a}_c,\mathbf{a}_s) \ . \tag{A1}$$

If we restrict ourselves to the interactionless case [which is a reasonable approximation since the turning points of $\beta(\rho_c)$ and $\beta(\rho_s)$ are not changed considerably for small ξ_1 and ξ_2] β_{SM} and β_{CF} can be computed from (12) and (18). By solving (12) numerically and choosing the larger of the two roots, we obtain $\rho^*_{c_{\max}}(\mathbf{a}_c)$ and after insertion into (11) $\beta_{\mathrm{CF}}(\mathbf{a}_c)$. The equivalent procedure for (18), for which the smallest root $\rho^*_{s_{\min}}(\mathbf{a}_s)$ must be found, leads to $\beta_{\mathrm{SM}}(\mathbf{a}_s)$. The final condition for MPC is then given by

$$\beta_s[\rho^*_{s_{\min}}(\mathbf{a}_s)] = \beta_c[\rho^*_{c_{\max}}(\mathbf{a}_c)] \ , \tag{A2}$$

where the subscripts indicate the different functional dependencies of β in (11) and (17).

[1] L. S. Bartell, E. J. Valente, and T. S. Dibble, J. Phys. Chem. **94**, 1452 (1990).
[2] T. S. Dibble and L. S. Bartell, J. Phys. Chem. **96**, 2317 (1992).
[3] T. L. Beck, J. Jellinek, and D. J. Wales, J. Chem. Phys. **87**, 545 (1987).
[4] D. J. Wales and R. S. Berry, J. Chem. Phys. **92**, 4473 (1990).
[5] J. Rose and R. S. Berry, J. Chem. Phys. **96**, 517 (1992).
[6] J. Jellinek, T. Beck, and R. S. Berry, J. Phys. Chem. **85**, 5943 (1986).
[7] T. L. Beck and R. S. Berry, J. Chem. Phys. **88**, 3910 (1988).
[8] M. Bixon and J. Jortner, J. Chem. Phys. **91**, 1631 (1989).
[9] R. S. Berry, Z. Phys. D **12**, 161 (1989).
[10] F. G. Amar and R. S. Berry, J. Chem. Phys. **85**, 5943 (1986).
[11] J. D. Honeycutt and H. C. Anderson, J. Phys. Chem. **91**, 4950 (1987).
[12] R. S. Berry, T. L. Beck, H. L. Davis, and J. Jellinek, in *Evolution of Size Effects in Chemical Dynamics, Part 2,* edited by I. Prigogine and S. A. Rice [Adv. Chem. Phys. **70**, 75 (1988), Pt. 2].
[13] R. S. Berry, P. Braier, R. J. Hinde, and H. P. Cheng, Isr. J. Chem. **30**, 39 (1990).
[14] J. E. Adams and R. M. Stratt, J. Chem. Phys. **93**, 1332 (1990).
[15] F. H. Stillinger and D. K. Stillinger, J. Chem. Phys. **93**, 6013 (1990).
[16] P. A. Braier, R. S. Berry, and D. J. Wales, J. Chem. Phys. **93**, 8745 (1990).
[17] H.-P. Cheng and R. S. Berrry, Phys. Rev. A **45**, 7969 (1992).
[18] J. P. Rose and R. S. Berry, J. Chem. Phys. **98**, 3246 (1993).
[19] J. W. M. Franken and J. F. van der Veen, Phys. Rev. Lett. **54**, 134 (1985).
[20] K. Strandburg, Rev. Mod. Phys. **60**, 161 (1988).
[21] F. F. Abraham and J. Q. Broughton, Phys. Rev. Lett. **56**, 734 (1986).
[22] P. Stolze, J. K. Nørskov, and U. Landman, Phys. Rev. Lett. **61**, 440 (1988).
[23] E. T. Chen, R. N. Barnett, and U. Landman, Phys. Rev. B **41**, 439 (1990).
[24] R. N. Barnett and U. Landman, Phys. Rev. B **44**, 3226 (1991).
[25] R. Lipowsky and W. Speth, Phys. Rev. B **28**, 3983 (1983).
[26] C. S. Jayanthi, E. Tosatti, and L. Pietronereo, Phys. Rev. B **31**, 3456 (1985).
[27] H. Löwen, T. Baier, and H. Wagner, Europhys. Lett. **9**, 791 (1989); Z. Phys. B **79**, 109 (1990).
[28] C. L. Briant and J. J. Burton, J. Chem. Phys. **63**, 2045 (1975).
[29] V. V. Nauchitel and A. J. Pertsin, Mol. Phys. **40**, 1341 (1980).
[30] P. Labastie and R. L. Whetten, Phys. Rev. Lett. **65**, 1567 (1990).
[31] S. Nosé, J. Chem. Phys. **81**, 511 (1983).
[32] S. Nosé, Mol. Phys. **52**, 255 (1984).
[33] H. L. Friedman, *A Course in Statistical Mechanics* (Prentice-Hall, Englewood Cliffs, NJ, 1985), Chap. 5.
[34] C. W. Gear, *Numerical Initial Value Problems in Ordinary Differential Equations* (Prentice-Hall, Englewood Cliffs, NJ, 1971).
[35] W. H. Press, B. P. Flannery, S. A. Teukolsky, and W. T. Vetterling, *Numerical Recipes* (Cambridge University Press, Cambridge, 1986), Chap. 10.
[36] T. Astakhova and R. S. Berry (unpublished).
[37] A. C. Mackay, Acta Crystallogr. **15**, 926 (1962).
[38] F. H. Stillinger and T. A. Weber, J. Chem. Phys. **81**, 5095 (1984).
[39] J. O. Hirschfelder, C. F. Curtis, and R. B. Bird, *Molecular Theory of Gases and Liquids* (Wiley, New York, 1954).
[40] M. E. Fischer and A. N. Berker, Phys. Rev. B **26**, 2507 (1982).
[41] Y. Imry, Phys. Rev. B **21**, 2042 (1980).

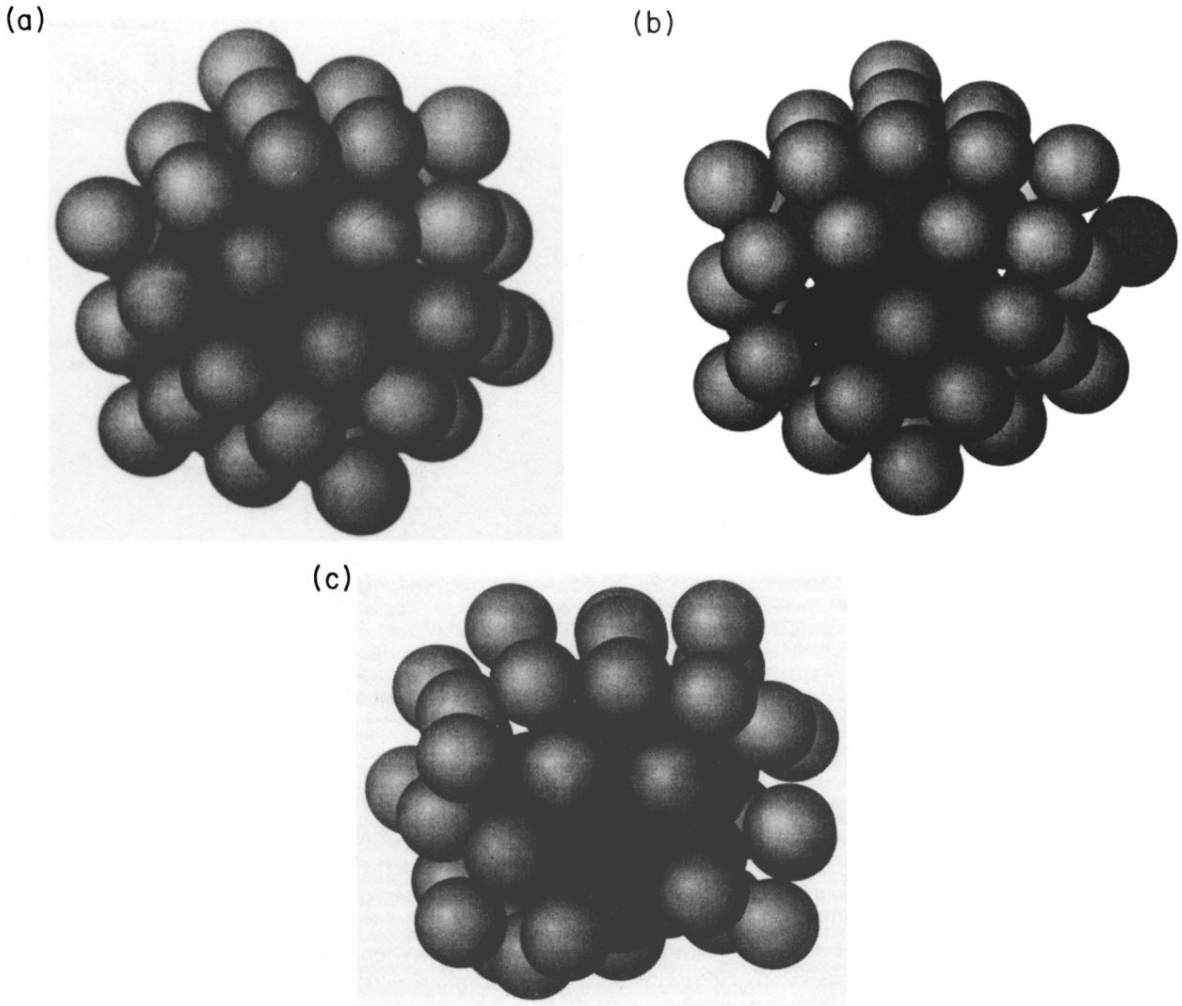

FIG. 3. Representative (quenched) structures of the coexisting phases in Ar_{55}: (a) solid icosahedral, $\phi = -5.292 \times 10^{-2}$ eV/atom, (b) surface melted with one floater, $\phi = -5.242 \times 10^{-2}$ eV/atom, and (c) homogeneously melted, $\phi = -5.027 \times 10^{-2}$ eV/atom. The core atoms and the floaters are represented by dark spheres, the outer shell atoms by light ones.